

Abstract

The study of aerosols in the troposphere and in the stratosphere is of major importance both for climate and air quality studies. Among the numerous instruments available, aerosol particles counters provide the size distribution in diameter range from few hundreds of nm to few tens of μm . Most of them are very sensitive to the nature of aerosols, and this can result in significant biases in the retrieved size distribution. We describe here a new versatile optical particle/sizer counter (OPC) named LOAC (Light Optical Aerosol Counter), which is light and compact enough to perform measurements not only at the surface but under all kinds of balloons in the troposphere and in the stratosphere. LOAC is an original OPC performing observations at two scattering angles. The first one is around 12° , and is almost insensitive to the nature of the particles; the second one is around 60° and is strongly sensitive to the refractive index of the particles. By combining measurement at the two angles, it is possible to retrieve accurately the size distribution and to estimate the nature of the dominant particles (droplets, carbonaceous, salts and mineral particles) in several size classes. This topology is based on calibration charts obtained in the laboratory. Several campaigns of cross-comparison of LOAC with other particle counting instruments and remote sensing photometers have been conducted to validate both the size distribution derived by LOAC and the retrieved particle number density. The topology of the aerosols has been validated in well-defined conditions including urban pollution, desert dust episodes, fog, and cloud. Comparison with reference aerosol mass monitoring instruments also shows that the LOAC measurements can be successfully converted to mass concentrations. All these tests indicate that no bias is present in the LOAC measurements and in the corresponding data processing.

9995

1 Introduction

The importance of measuring the concentration and size distribution of aerosols in the lower atmosphere has been highlighted by various studies. For instance, their presence in ambient air can have direct effects on human health (e.g. Zemp et al., 1999; Brunekreef and Holgate, 2002), and their interaction with solar radiation and clouds are affecting regional and global climate (Ramanathan et al., 2001; Diner et al., 2004; Kanakidou et al., 2005; Quaas et al., 2008). When very high concentrations of ashes after volcanic eruptions are present at cruise altitude, they can affect air traffic (e.g. Chazette et al., 2012). In the middle atmosphere, aerosols play a significant role in stratospheric chemistry through heterogeneous reactions with nitrogen and halogen species (e.g. Hanson et al., 1994, 1996), and they can affect climate through their role in the global radiative balance of the Earth (e.g. Hansen et al., 1992; Ammann et al., 2003). The concentration and size of the particles are highly variable due to the large variety of aerosol sources and properties, both of natural and man-made origin, and because of their relatively short residence time in the atmosphere. To understand and predict aerosol impacts, it is important to develop observation and monitoring systems allowing for their full characterization.

Instruments have been developed for routine measurements or for dedicated campaigns. Observations can be conducted from the ground, from unmanned aerial vehicles (UAV), from aircrafts, from balloons, and from satellites. To retrieve the physical properties of the aerosols, it is necessary to combine the information obtained with different instruments. In situ mass-spectrometers (Murphy et al., 2007) and aerosol collecting instruments (Brownlee, 1985; Blake and Kato, 1995; Allan et al., 2003; Bahreini et al., 2003; Ciucci et al., 2011) provide their composition. Optical instruments performing remote sensing measurements from the ground or from space with photometric, lidar, and extinction techniques (Shaw et al., 1973; Dubovik and King, 2000; Bitar et al., 2010; Winker et al., 2010; Salazar et al., 2013) provide indications on the size distribution and on the nature of the particles (liquid, carbon, minerals, ice, ...), generally

9996

assuming a priori hypotheses in the retrieval process. Complementarily, in situ optical measurements with optical particle counters can provide more accurate information on the size distributions of the particles.

5 The present study deals with optical aerosol particles counters (OPCs). The corresponding measurement principle relies on the properties of light scattered by particles injected in an optical chamber and crossing a light beam (e.g. Grimm and Eatough, 2009). The measurements are usually conducted at “large” scattering angles, typically around 90° with collecting angle of a few tens of degrees. At such angles, the light scattered is depending both on the size of the particles and on their refractive index. Conventional counters are calibrated using latex and glass beads and are post-calibrated using Mie calculations (Mie 1908) for liquid aerosols (the refractive index of latex beads and liquid aerosols is well known, assuming no imaginary part of the index i.e. non-absorbing aerosols). Some instruments can be also be post-calibrated for the observation of specific particles, as desert dust or urban pollutants, assuming a given value of their refractive index.

10 The refractive index dependence can be partially determined by performing measurements at different scattering angles, since the variation of the scattered intensity with scattering angles is strongly dependent on the refractive index of the particles (Volten et al., 2006; Francis et al., 2011). Thus, performing simultaneous measurements at different angles can provide an indication of the nature of the particles. Such an approach was used by Eidhammer et al. (2008) at angles of 40° and 74° mainly for the identification of mineral particles, and by Gayet et al. (1997) with a ring of detectors covering the whole scattering angle range for the identification of cloud droplets and icy particles.

15 Another approach was proposed by Renard et al. (2010a); in this case, measurements are conducted at small scattering angles, below 20° , where the light scattered is less sensitive to the refractive index of the particles. In this angular region, the scattered light is dominated by diffraction (which is not sensitive to the refractive index), at least for irregular grains as those found in the atmosphere. Such non-dependence of

9997

the refractive index was confirmed by measurements conducted at a scattering angle around 15° for different types of irregular grains (Lurton et al., 2014). In this case, the light scattered is dependent only on the size of the particles, allowing a better determination of the corresponding size distribution. However, the main problem of measurement at small angles is stray-light contamination. Thus a real-time correction of this signal offset due to the stray-light, which can vary with time, must be developed.

5 Aerosol particles counters are often used on the ground; some of them are used in the free atmosphere on-board aircraft or large balloons during dedicated campaigns, for example for the studies of desert dust events or volcanic aerosols (Bukowiecki et al., 2011; Jégou et al., 2013; Ryder et al., 2013) or for stratospheric studies (Rosen, 1964; Ovarlez and Ovarlez, 1995; Deshler et al., 2003; Renard et al., 2008, 2010b). We propose here a new optical particle counter concept, called LOAC (Light Optical Aerosol Counter) that is light and compact enough to perform measurements on the ground and under all kinds of balloons in the troposphere and in the stratosphere, including meteorological balloons. LOAC uses a new approach combining measurements at two scattering angles. The first one is around 12° , an angle for which scattering is weakly sensitive to the imaginary part of the refractive index nature of the aerosols, allowing the retrieval of the particle size distribution. The second one is around 60° where the light scattered is strongly sensitive to the refractive index of the particles, and thus can be used to evaluate their topology (liquid droplet are transparent, minerals are semi-transparent, and carbonaceous particles are strongly absorbing).

15 In this first paper, we will present the principle of measurements and calibration, and cross-comparison exercises with different instruments that detect atmospheric aerosols. In the companion paper, we illustrate first scientific results from airborne observations on-board balloons and unmanned aircraft (Renard et al., 2015).

9998

2 Principle of measurements

2.1 Instrument concept

LOAC is a modular instrument, for which some parts can be changed depending on the measurements conditions. For measurements under balloon or on the ground in low wind conditions, the aerosols are collected by a metal profiled inlet designed to optimize the sampling conditions when oriented in the wind direction. The particles are drawn up to the optical chamber, through an isostatic tube and to the injector that focusses the flux inside the laser beam. LOAC uses a small vane-type pump (having a life-time of 3 weeks in continuous operation) working at $\sim 2 \text{ L min}^{-1}$. The pump is connected to the exit of the optical chamber by a flexible plastic tube. The optical chamber is open, thus the pressure is the same as outside. In-flight tests under sounding balloons have shown that the rotation speed of the pump is not affected by pressure variations.

For measurements in windy and rainy conditions, the inlet can be replaced by a total suspended particulate or TSP inlet rejecting rain droplets and particles greater than $100 \mu\text{m}$. For long-duration measurements, the small pump can be replaced by a robust pump; to maintain the aerosol detection efficiency, the pump flux must be in the range $1.3\text{--}2.7 \text{ L min}^{-1}$.

To minimize its weight, the optical chamber is in plastic Delrin[®]. The weight, including the pump, is of 300 g. The electric consumption is of 340 mA under 8 V (which corresponds to a power of 3 W). The optical chamber and the pump can fit in a rectangle box of about $20 \text{ cm} \times 10 \text{ cm} \times 5 \text{ cm}$.

LOAC is mainly designed for the detection of irregular grains, as those present in the ambient air (Fig. 1, from Institute of Physics of the University of Sao Paulo, Brazil). It uses a statistical approach for the size and concentration retrievals, as done for the laboratory PROGRA2 instruments dedicated to the study of optical properties of irregular levitating grains (Renard et al., 2002). Because of their shape, their orientation and their rotation in the air flow, the scattering properties of an individual grain vary with time at a given scattering angle (this variation could be more than a factor 2, as shown

9999

during laboratory tests by photodiodes and imagery measurements with PROGRA2). This must be taken into account for the calibration and data analysis. Thus, we propose here a calibration approach that can differ from the one used for other optical counters.

The sampled air crosses a laser beam of 25 mW working at the wavelength 650 nm. The homogeneity of the beam is of $\pm 20\%$. The scattered light is recorded by two photodiodes at scattering angles respectively in the $12\text{--}16^\circ$ (hereafter called the 12° channel) and $55\text{--}65^\circ$ (hereafter called the 60° channel), as shown on Fig. 2. Instead of using lenses to collect the light, the photons travel directly to the photodiodes through pipes, providing fields of view with a few degrees. The collecting area of the photodiodes is larger than the diameter of the pipes. This system prevents optical misalignment problems in case of vibrations and strong temperature variations like those encountered during atmospheric balloon flights. Such a concept of scattering measurements without collecting lenses was tested and validated by Daugeron et al. (2007).

The electronic sampling is at 40 kHz and the transit time of particles inside the laser beam is equal or lower than $500 \mu\text{s}$. As said before, stray light contamination is high at small scattering angles and needs real-time correction. The stray light correction method presented in Renard et al. (2010a) was applied to the LOAC measurements. The stray light acts as a flux continuum, which can slightly vary over time due to changes in the temperature and pressure conditions and possible dust contamination in the optical chamber. The light scattered by the particles is superimposed on this continuum, which can be assumed as a continuous base-line over a short time interval. This baseline is determined before and after the intensity pulse produced by the particles that cross the laser beam.

The maximum of the intensity pulse is obtained after subtracting the stray-light contamination. Figure 3 presents an example of real ambient air measurements of the time evolution of the flux scattered by a $5 \mu\text{m}$ particle and by few submicronic particles. The pulse is slightly asymmetric, because the particles decelerate when crossing the optical chamber. This deceleration occurs because the diameter of the optical chamber is larger than the diameter of the inlet; thus the particles encounter pressure relaxation.

Some secondary flux maxima may be present in the pulse and can be attributed to the rotation of irregular shaped particles in the air flow. The search for a new intensity peak is inhibited until the flux decreases to a given threshold, represented in Fig. 3 by the red line. This procedure prevents multiple counting of the same particle (of irregular shape) that exhibits secondary flux maxima.

This pulse analysis is performed by the on the on-board electronics, which provides every 10s the concentrations detected by the 2 channels. Until now, an additional computer has been necessary to record and analyse the data.

2.2 Calibration

The calibration of an optical counter is not an easy task, especially for the detection of irregular particles (Whitby and Vomela, 1967; Gebhart, 1991; Hering and McMurry, 1991; Belosi et al., 2013). A first presentation of the calibration procedure for measurements at small scattering angles using a LOAC optical chamber can be found in Lurton et al. (2014).

Only the 12° channel, which is insensitive to the refractive index of the particles, must be calibrated. The 60° channel will be used as a comparison to the 12° channel measurements to determine the typology of the aerosol, as explained in the Sect. 2.4.

Monodisperse latex beads, which are perfect transparent spheres, have been used for diameter calibration in the 0.2–4.8 μm range; glass beads have been used at 5 μm (see Figs. 2 and 3 of the Lurton et al., 2014 paper for the LOAC response to monodisperse beads). In fact, Mie calculations show that the scattered flux encounters strong oscillations linked to small changes both in diameter and in scattering angle. Conventional aerosol counters use large field of view, typically a few tens of degrees, to average these oscillations. On the opposite, the LOAC 12 and 60° measurement channels have a field of view only of few degrees and use no lens. The detected flux at the 12° channel is then very sensitive to the position of the individual bead inside the laser beam, and thus to its scattering angle. Taking into account this constraint, we

10001

considered here only the highest flux scattered by each size class of monodisperse beads.

The electronic noise is lower than 20 mV at ambient temperature and lower than 10 mV at low air temperatures. Statistically speaking, the noise is divided by the root mean square of the number of identical measurements (here the number of events detected in a given size class). To reach a 1 mV accuracy in case of 20 mV noise, which is necessary to be able to discriminate the smaller size classes and to establish accurately the size distribution, at least 20×20 (= 400) particles must be detected for each size class.

During laboratory calibration, it is easy to reach such concentration levels using monodisperse beads. During real measurements inside the atmosphere, we must ensure that such particle concentrations are indeed present for all size classes below 1 μm. The LOAC has an integration time of 10 s, with a pumping flow of about 2 L min^{-1} . Even in low polluted ambient air at ground (“background conditions”), all counting instruments have shown in the past that concentrations are greater than 1 particle cm^{-3} for size classes smaller than 0.5 μm (having a 0.1 μm width), which corresponds to $2000/6$ = more than 300 particles during the 10 s LOAC integration time. For particles in the 0.5–1 μm size classes (having a width of 0.1 or 0.2 μm), concentrations are greater than 0.1 particle cm^{-3} , giving more than 30 particles per size class.

For all the cross-comparison exercise presented below, the measurements were integrated from 2 to 15 min. For the 2 min integration time, the number of particles given above must be multiplied by 12, giving are at least 3000 for the 3 first size classes and 300 for the other ones. For a 15 min integration time, these numbers must be multiply again by 7.5. Thus, the LOAC class identification can be conducted with the expected accuracy in the ambient air. Obviously, in case of polluted air, all these values could be also 2 to 3 orders of magnitude higher (1000 particles cm^{-3} between 0.2 and 0.3 μm is often encountered).

In case of very low particle concentrations, as those that can be encountered during flights in the stratosphere with typically less than 1 particle cm^{-3} greater than 0.2 μm,

10002

the size attribution will be less accurate. Thus, the retrieved size distributions and the time-evolution of the concentration will be more scattered and need to be averaged in altitude.

For the calibration in the 7–45 μm size range, different natures of irregular grains have been used: carbon particles, dust sand of various types, ashes and salts (see for example Fig. 4 of the Lurton et al., 2014 paper). The size selection was obtained using sieves. For diameters at $\sim 90 \mu\text{m}$, calibrated silicon carbide grains were used, the size being characterised by the provider. The diameter presented here corresponds to an equivalent (or optical) diameter, which can differ significantly from the aerodynamic diameter or from the electric mobility diameter used by non-optical instruments for ambient air measurements. Several tens of grains are necessary to ensure a mean random orientation, to be able to derive a mean equivalent diameter. The relation between flux and size was derived by considering the diameter where the concentration distribution is at its maximum. The measurements with different nature of grains confirms that no significant dependence with the particle type exists for the variation of the scattered flux with their diameter, as presented in Fig. 8 of Renard et al. (2010a) and Fig. 5 of Lurton et al. (2014).

Taking into account the laser departure from homogeneity, the electronic noise, and the statistical approach, the uncertainties in size calibration is of $\pm 0.025 \mu\text{m}$ for particles smaller than $0.6 \mu\text{m}$, 5 % for particles in the $0.7\text{--}2 \mu\text{m}$ range, and of 10 % for particles greater than $2 \mu\text{m}$. Figure 4 presents the calibration curve for the 12° channel, where the scattered flux is given in mV, which corresponds to the photodiode output voltage (updated from Lurton et al., 2014). The offset due to the electronic dark current and high frequency noise of the detector were added to the calculations; thus the curve asymptotically decreases with decreasing size to this offset value.

The calibration with the latex beads captures well the large-amplitude Mie oscillations up to $5 \mu\text{m}$ in diameter, calculated by integrating the scattered fluxes over the whole LOAC field of view ($12\text{--}16^\circ$). In particular, the amplitude of the oscillations at 1, 2 and $5 \mu\text{m}$ are well reproduced. For the larger sizes, calibrated with irregular grains, the

10003

evolution of the scattered flux with size is lower than the one expected from the Mie calculation. This difference was attributed to the natural roughness of the particulates and the small LOAC field of view, as shown by theoretical calculations (Lurton et al., 2014). It was found that a relatively small roughness parameter caused the scattered intensities to collapse on a lower saturation limit corresponding solely to the diffraction part of the scattered light.

Solid particles found in ambient air are not perfectly spherical and have some irregularity on their surface, even for the sub-micrometre (sub- μm) sizes (e.g. Xiong and Friedlander, 2001; McDonald and Biswas, 2004). Thus, the Mie oscillations will disappear and the scattered flux will roughly cross the middle of the oscillations amplitude (except perhaps for some iced crystals encountered in some clouds). A good illustration of the light scattering properties by irregular grains can be found in Weiss-Wrana (1983).

The flux evolution with diameter for the particles larger than a few μm can be fitted using a power law. As the lower saturation limit of Lurton et al. (2014) is likely to exist even for very slightly rough particulates, this power law can be reasonably used to estimate the sizes of any sort of real particulates found in the atmosphere. The best fit is obtained using a power law in $D^{-1.0}$ (adding an offset of 17 mV) where D is the particle diameter, as shown in Fig. 4.

Such an approach is validated by performing measurements with particles in urban air, as shown in Fig. 5. Measurements were integrated over 15 min (90 acquisitions of 10 s). LOAC captures well the continuous decrease of concentration with increasing size, as previously established by various kinds of instruments, such as electrostatic low pressure impactors (e.g. Shi et al., 1999). A calibration error would produce oscillations in the size distribution, correlated to the Mie oscillations. On the other hand, we would expect that the LOAC calibration could be inappropriate for droplets, which are supposed to be perfectly spherical. In fact, such a phenomenon was not observed during laboratory tests conducted for droplets only, nor during measurements inside fog and clouds. We can expect that droplets are slightly distorted when entering the optical

10004

chamber due to changes in the air flow speed between the aerosols injector and the optical chamber.

Thus, the LOAC detection size range is between 0.2 and $\sim 100 \mu\text{m}$. LOAC, with its present calibration procedure, is operated to the detection of irregular grains and droplets, but not to perfect spherical solid grains, such as latex or metal beads for which uncertainties arise from the smoothing of Mie oscillations by the calibration curve (in this case, the total concentration is correct but the size attribution can be erroneous).

Overall, a total of 19 size classes are defined for diameters between 0.2 and $100 \mu\text{m}$ (Table 1). The upper limit can be lower, however, depending on the sampling collection cut-off of the inlet. The size classes are chosen as a good compromise between the instrument sensitivity and the expected size distribution of ambient air aerosols.

2.3 Concentration measurements

Counting is conducted while the particles cross the laser beam one by one, and are classified in size classes corresponding to the scattered flux. The measurements are integrated during 10 s and are converted to number densities or particles cm^{-3} . The detectors of the two channels (12 and 60°) work asynchronously.

This discrete detection works well for large particles greater than $2 \mu\text{m}$, with uncertainty in size attribution of 10 %. For smaller particles, the size determination is within the calibration errors bars ($\pm 0.025 \mu\text{m}$ for particles smaller than $0.6 \mu\text{m}$, 5 % in the $0.7\text{--}1 \mu\text{m}$ range) if more than 400 particles are detected for each size classes.

The optical and electronic response of the system has been modelled by a numerical Monte-Carlo method, taking into account the shape of the laser beam, the speed of the particles inside the laser beam and the instrument noise. To ensure a good statistical approach, 10^4 particles were randomly injected for each size class. The ratio of the number of detected particles over the number of injected particles provides the detection efficiency. For the smallest particles, only the brightest part of the peak of the pulse of the scattered flux is observable and the apparent transit time in the laser beam is a few tens of μs (in Figs. 3 and 4 small peaks are present). Thus, some par-

10005

ticles cannot be detected. The detection efficiency increases as the diameter of the particles increases, and is reaching 100 % for particles larger than $1 \mu\text{m}$. The concentrations of submicron size particles are then corrected using these detection efficiency coefficients.

For particles larger than $1 \mu\text{m}$, the observed transit time in the laser beam is at its maximum ($\sim 500 \mu\text{s}$) and the expected maximum concentration is of about 20 particles cm^{-3} . In fact, even higher concentrations can be determined using a statistical approach when several particles cross the laser beam almost simultaneously. The higher are the concentration, the lower is the probability that the scattered intensity peaks decreases below the threshold to start a new counting. In this extreme case, the real concentrations are inversely proportional to the detected concentrations. Another Monte-Carlo numerical modelling was conducted to establish the relationship between the number of particles $> 1 \mu\text{m}$ detected and the number of particles injected in the laser beam (Fig. 6). In the simulations, particles were randomly injected (in time), with concentrations increasing from 0 to 500 particles cm^{-3} by step of 1 particle cm^{-3} . The response is almost linear up to 10 particles cm^{-3} , reaching a kind of saturation value at around 15 particles cm^{-3} , and decreases for larger concentrations. It is obvious that such a corrective procedure must be used only in dense aerosol media (more than 10 particles greater than $1 \mu\text{m}$ cm^{-3}), as fog or clouds, i.e. in conditions which must be confirmed by independent measurements. At present, this procedure is applied only when large droplets are detected by LOAC using the topology procedure presented below. In this case, up to 200 large particles cm^{-3} can be detected.

For the smaller particles, the signal of the scattered flux is close or inside the noise. The photodiodes cannot detect the whole transit of the particles inside the laser beam, but just the brighter part of the peak. Thus, the effective acquisition time can be reduced down to $35 \mu\text{s}$ instead of around $500 \mu\text{s}$ for the largest particles. Then, a greater number of particles can be detected. Taking into account also the detection efficiency for the smaller particles, up to 3000 particles cm^{-3} can be (statistically) detected.

For the LOAC integration time of 10 s, the counting uncertainty can be derived from the Poisson counting statistics. This uncertainty, defined as the relative standard deviation, is 60 % for aerosol concentrations of 10^{-2} cm^{-3} , 20 % for 10^{-1} cm^{-3} , and 6 % for concentrations higher than 1 cm^{-3} . Such uncertainties can be reduced by averaging the concentration measurements for each size classes or by increasing the integration time. Nevertheless, such calculation does not take into account the real instrumental uncertainties dominated by the electronic noise and the inlet sampling efficiency.

LOAC is designed to be used in various atmospheric conditions. The temperature can dramatically change, in particular during balloon flights up to the middle stratosphere. The electronics offset can change with time because of the sensitivity of the electronic components to atmospheric temperature variations. The instrument performs a check of its noise level after 10 min of measurements. If the noise differ by more than 50 % from the previous check, an electronic re-calibration is automatically performed to estimate the offset variation and to adjust the calibration. A processing software is applied after the experiment to check the offset time-evolution during the 10 min periods and to then correct the raw measurements.

2.4 Aerosols typology

The scattered flux recorded at 60° is very sensitive to the refractive index of the particles and thus to their nature (as said before this phenomenon appears at scattering angles greater than $\sim 20^\circ$). The more absorbing they are, the lower the recorded fluxes. Thus, we use the “ 60° channel” as a diagnostic for the effect of the refractive index on the scattered fluxes. This channel uses the same flux threshold (in mV) as the 12° channel, in order to perform a direct comparison of the counting detected by two channels. For a given size class and for a given particle concentration recorded in the 12° channel, the concentration detected by the 60° channel decreases when the imaginary part of the refractive index increases. This increase of the imaginary part leads to an underestimation of the real size of the particles, and thus produces a diameter bias in the size distribution (diameter vs. concentration) for the 60° channel with respect to the

10007

12° channel. An example of the procedure used to determine this effect is presented in Fig. 7, where the size distributions of the two channels are presented. For a given particle size of the 12° channel (noted D1), we consider the concentration value of the 60° channel. Then we search for the same concentration value on the 12° channel (a linear interpolation is used if needed). The corresponding diameter is then determined (D2). Finally, we define a so-called “speciation index” as the ratio D2/D1. The more absorbing the particles are, the higher this ratio. This procedure is conducted for each size class.

This procedure works well for irregular particles, but not for solid symmetrical particles; in this later case, the Mie oscillation will produce strong fluctuations in the evolution of the speciation index with size (we have indeed observed this effect inside some cirrus clouds). Also, this procedure must be used only for a large enough number of detected particles per size class, because of the irregular shape of the particles. Laboratory tests have shown that about 20 particles in a size class are sufficient to be able to indicate the aerosol topology. In its nominal operating mode, LOAC provides the speciation index every 1 min. For the analysis of continuous ground-based measurements presented below, we have conducted the topology detection with an integration time of 15 min (assuming that the aerosols are stationary).

Different types of particles have been tested in the laboratory to assess the amplitude of the speciation index throughout the measurement size range: organic carbon, black carbon, desert dust or sand from different origins (excluding black sand), volcanic ashes, plaster, salt (NaCl), water droplets, droplets of mixture of water and sulphuric acid. They can be classified in 4 families: carbonaceous particles, minerals, salts and liquid droplets. Figure 8 presents the curves obtained in laboratory for the various samples. Then, “speciation zones” charts (speciation index vs. real diameter) are defined by the minimum and maximum speciation index values reached by each family, taking into account the measurement uncertainties. Among solid particles, carbonaceous particles produce the higher speciation index and salt the lower, mineral particles being in between. Detailed analysis has shown that most of the carbon particles are in the

10008

specific studies where very large particles dominate, as measurements inside fog or clouds, or because of mechanical constraint if a TSP inlet cannot be mounted, the particles can be collected by a tube having a bevelled metal inlet and oriented downwards. In this case, the largest particles are generally under-sampled and a corrective coefficient must be applied, taking into account the direction and the speed of the wind.

For measurements under balloons floating at constant altitude, the relative speed between ambient air and the inlet is close to zero. The sampling efficiency assessed using the Agarwal and Liu (1980) criterion for an upward-facing inlet shows that the sampling is unbiased for particle with diameter below $20\ \mu\text{m}$.

The sampling line used during the flights is composed of a thin wall metallic probe and antistatic tubing. The thin wall aerosol probe has an inlet diameter equal to $5.4\ \text{mm}$ and is connected to a tube of about $20\ \text{cm}$ long and $6.7\ \text{mm}$ internal diameter. The sampling line is connected vertically to the LOAC. Nevertheless, due to the tube stiffness, the line can be inclined with a maximum sampling angle of 30° from vertical. The sampling efficiency of the line was assessed using modelling calculations in order to account for changes in atmospheric pressure, temperature and possible changes of the probe orientation during these flights. For that purpose, the values of pressure and temperature as a function of altitude are taken from the international standard atmosphere. Sampling efficiency calculations have been made by considering a balloon ascending velocity of $5\ \text{m s}^{-1}$, a LOAC sampling flow rate equal to $1.7\ \text{L min}^{-1}$ and two angles of the sampling line from the vertical (0 and 30°). According to these parameters, the inlet aspiration velocity of the probe is equal to $1.24\ \text{m s}^{-1}$ (sub-isokinetic) and the flow is laminar in the tubing for all altitudes.

The mechanisms considered to calculate the sampling efficiency are the inlet efficiency of the probe in isoaxial and isokinetic sampling conditions (Belyaev and Levin, 1974; Hangal and Willeke, 1990) and particle losses in the tubing due to gravitational settling when the line is not perfectly vertical (Heyder and Gehbart, 1977). Calculations have been conducted for particles with diameter ranging from 0 to $20\ \mu\text{m}$, and from the ground to an altitude of $30\ \text{km}$. Figure 9 presents the sampling efficiency for a 0°

10011

deviation (isoaxial) and for a 30° deviation of the sampling line with respect to the vertical. Data are plotted according to the particle aerodynamic diameter which describes particle settling and inertia phenomenon.

In isoaxial conditions, results show for all altitudes an increase of sampling efficiency with the particle diameter, up to a factor > 3 for the largest particles. In this case, there is no particle deposition in the sampling line and the sampling is dominated by sub-isokinetic conditions (apparent wind velocity higher than inlet probe velocity). A sampling efficiency higher than unity is explained by the particle inertial effect resulting from the divergence of the flow field at the inlet of the probe. The increase in sampling efficiency with altitude is due to changes in air viscosity and gas mean free path with temperature and pressure.

When the tube is inclined by 30° from the vertical, the sampling efficiency is between 1 and 2. The sampling efficiency is lower than for the 0° isoaxial conditions. Firstly, the sub-isokinetic effect is reduced by the orientation of the tube, and secondly, deposition can occur in the tubing due to particle settling.

Since the tube always has a deviation of about 30° during the balloon flights, we consider only the results at 30° from the vertical. The over-sampling effect is negligible for particles smaller than $5\ \mu\text{m}$ up to the lower stratosphere and for particles smaller than $2\ \mu\text{m}$ in the middle stratosphere. Thus, this effect will just affect the retrieved concentrations of the largest particles.

The results of these theoretical calculations are not yet fully validated by an experimental approach with LOAC itself. Thus, all balloon measurements in the stratosphere will not be corrected from this aerodynamic effect. It could be taken into account in future work involving large particles, for example when converting concentrations to extinction by comparison with remote sensing instruments, or to estimate the real concentration of the interplanetary dust in the middle atmosphere.

10012

where D_{\min} and D_{\max} are the lower and upper diameter of a given size class, respectively. With such a formula, the mean volumetric diameter is at about 60 % of the size class width instead of 50 % for the mean geometric diameter. For each size class, the volume of the particles is calculated assuming sphericity. To be consistent with the AERONET data, the LOAC results are presented in radius instead of diameter.

Figure 16 presents two examples of comparison between LOAC and AERONET size distributions for two different amounts of sand particles in the troposphere (the contribution of the stratospheric particles is negligible). The bi-modal distribution is typical for a desert dust or sand plume event. The two instruments are in excellent agreement, both in size distribution and volume concentrations. It is worth noting that the volume concentrations are proportional to the cube of the size of the particles, an error in the LOAC calibration would lead to strong discrepancies, which is not the case.

The cross-comparison measurements presented above have been conducted for different air temperature, including day-night cycles and seasonal temperature variations. No effect of the temperature on the accuracy of the retrieved concentrations has been pointed out. These results confirm that the LOAC real-time noise-checking process works well.

All these cross-comparison exercises have shown that the LOAC measurements are consistent with those of the other instruments considered here, accounting for the errors and the limitation of the various techniques. This confirms that no systematic bias are present in the LOAC calibration and in the data analysis when LOAC is used at ground.

3.2 Tropospheric vertical distribution

Cross-comparison exercises have been also conducted for balloon-borne LOAC measurements.

LOAC has performed tropospheric flights during the ChArMEx campaign from Minorca Island in time-coincidence with the WALI aerosols lidar measurements (Chazette et al., 2014) at a few tens of km apart. One LOAC flight was conducted under meteorological

10017

balloon on 16 June 2014; two LOAC flights were conducted on 19 June 2013 at the same time, the first one being under a meteorological balloon and the second being under a pressurized tropospheric balloon (see the companion paper for more information of the balloons and the gondolas, Renard et al., 2015). To be compared to lidar extinction data at 350 nm, the LOAC data were converted to extinction using Mie scattering theory, assuming spherical sand particles having an refractive index of $n = 1.6 + 0.05i$ (such index is an average of values available in the literature). Uncertainties of the refractive index values are included in the errors bars calculations of the retrieved LOAC extinctions. Figure 17 presents the tropospheric vertical profile of LOAC and WALI lidar extinctions. Taking into account the instrumental errors bars, LOAC and WALI have captured the same main vertical structures and the extinction values are in average in good agreement in the lower troposphere.

3.3 Topology of the particles

The speciation zones, obtained from laboratory measurements, must be validated in real atmospheric conditions.

Urban ambient air measurements are proper for the detection of carbon particles (black and organic carbon), especially during well-identified pollution events. Permanent LOAC measurements have been conducted at "Observatoire Atmosphérique Generali" (OAG) in the South-West of Paris since May 2013 (48.841° N, 2.274° E). This observatory is a recreational tethered balloon operated in a public park; the LOAC measurements nominal maximum altitude is 120 m but some flights could be conducted up to an altitude of 270 m. The measurements can be sorted out between measurements with the balloon at ground level and measurements during flight. Figure 18 presents an example of light absorbing particles (probably carbonaceous ones) detected at the OAG on 29 December 2013 around 07:30 UT. In this example, the speciation index curve is well inside the carbon speciation zone in the whole size range up to $\sim 10 \mu\text{m}$.

In addition to sounding balloons mentioned above, measurements under drifting balloons launched from Sant Lluís on Minorca Island were also conducted during sev-

10018

eral well-identified desert dust events above the Mediterranean sea during the summer ChArMEx campaign. Figure 19 presents an example on 17 June 2013, around 14:30 UT (approximate balloon position: 41.9° N, 4.1° E) at an altitude of 2050 m under a low altitude pressurized drifting balloon. The speciation curve is well inside the mineral dust zone, showing that LOAC has indeed detected the desert dust event.

Measurements in the marine atmospheric boundary layer were also conducted with a low altitude balloon on 22 July 2013 drifting in an altitude range of 250–400 m, launched from the French Levant Island off Hyères on the Mediterranean French coast (43.021° N, 6.461° E). Figure 20 presents the measurements at 21:25 UT (approx. balloon position: 43.0° N, 6.55° E, alt. ~ 275 m), and the topology is mainly in the “salt zone”, as expected for a measurement close to the sea surface.

Droplet topology was validated in fog events during the ParisFog campaign; but also during cloud measurements conducted in May 2013 at the Puy de Dôme observatory (45.772° N, 2.964° E, alt. 1465 m). Figure 21 presents an example of measurements inside a cloud on 15 May 2013 at 10:30 UT. Globally, the topology identification is inside the droplets zone, which indicates that all of the particles were indeed liquid. In addition, measurements were conducted inside haze or thin cloud at an altitude of 1.2 km during a flight under a meteorological balloon launched from Reykjavik, Iceland (64.127° N, 21.904° W), on 7 November 2013 at 12:30 UT in the frame of the VOLTAIRE-LOAC campaign for the study of the stratospheric aerosol trend. The presence of the droplets was confirmed by the on-board humidity sensor, with a hygrometry of 90 %. The topology in Fig. 22 is well inside the droplets zone.

Finally, most of the measurements under meteorological balloons in the middle atmosphere show that (pure) liquid water and sulphuric acid droplets largely present in the stratosphere are close to the lower part of the droplets zone, and sometimes slightly below. Vertical profiles of LOAC concentration and topology measurements are presented in the second part (Renard et al., 2015).

These examples show that the topology determination works well in case of homogeneous aerosol media. Nevertheless, there are two limitations of this process. First,

10019

the analysis of measurements conducted in heterogeneous media could be difficult or even inaccurate, in particular when different size modes are present. In this case, the speciation curve exhibits unusual oscillations that match none of the speciation zones. Secondly, some high porosity aerosols can exhibit high values for the speciation index, even if they are not black (as fluffy silica). Then, the topology determination is providing most of the time the nature of the particles, but one has to be cautious in the analysis when the speciation curves are non-typical.

3.4 Mass concentrations

Our final test to evaluate both the calibration of LOAC and the retrieval of concentrations in all size classes (but especially large particles) is to convert the number size distribution measurements to mass concentrations and to compare the results to reference mass measurements. This is the most sensitive test to evaluate LOAC, since mass concentrations are proportional to the cubic diameter of the particles (and to their density). The topology helps to determine the type of aerosols, from which a density can be deduced. The density determination is necessary for the conversion of number concentrations (in cm^{-3}) to mass concentrations (in $\mu\text{g m}^{-3}$).

Measurements were conducted first in indoor air (in the “pollution room” at the LPC2E laboratory) in autumn 2013, by injecting in the air of the room different kinds of carbonaceous and mineral particles (smaller than 20 μm) in various concentrations to produce a large range of mass concentrations. The reference mass measurements were achieved with a calibrated TEOM microbalance. An air flow system was used (when needed) to prevent sedimentation of the particles in the room. Also, some measurements have been conducted without injecting particles, to detect only the smallest particles present in the ambient air, in particular during the night without convection in the room.

The volume concentration is calculated for each size class, using the mean volumetric diameter, assuming spherical particles, and is multiplied by the corresponding concentrations. The mass concentration is obtained by multiplying these results by the

10020

- Vignati, E., Stephanou, E. G., and Wilson, J.: Organic aerosol and global climate modelling: a review, *Atmos. Chem. Phys.*, 5, 1053–1123, doi:10.5194/acp-5-1053-2005, 2005.
- Lurton, T., Renard, J.-B., Vignelles, D., Jeannot, M., Akiki, R., Mineau, J.-L., and Tonnelier, T.: Light scattering at small angles by atmospheric irregular particles: modelling and laboratory measurements, *Atmos. Meas. Tech.*, 7, 931–939, doi:10.5194/amt-7-931-2014, 2014.
- McDonald, R. and Biswas, P.: A methodology to establish the morphology of ambient aerosols, *J. Air Waste Manage.*, 54, 1069–1078, 2004.
- Mie, G.: Beiträge zur Optik trüber Medien, speziell kolloidaler Metallösungen, *Annal. Phys.*, 3, 377–445, 1908.
- Murphy, D. M., Cziczo, D. J., Hudson, P. K., and Thomson, D. S.: Carbonaceous material in aerosol particles in the lower stratosphere and tropopause region, *J. Geophys. Res.*, 112, D04203, doi:10.1029/2006JD007297, 2007.
- Ovarlez, J. and Ovarlez, H.: Water vapour and aerosol measurements during SESAME, and the observation of low water vapour content layers, Proc. Third European Workshop Polar Stratospheric Ozone, Schliersee, Germany, 18–22 September 1995, *Air Pollution Rep.* 56, edited by: Pyle, J. A., Harris, N. R. P., and Amanatidis, G. T., European Commission, 205–208, 1995.
- Quaas, J., Boucher, O., Bellouin, N., and Kinne, S.: Satellite-based estimate of the direct and indirect aerosol climate forcing, *J. Geophys. Res.*, 113, D5, doi:10.1029/2007JD008962, 2008.
- Ramanathan, V., Crutzen, P. J., Lelieveld, J., et al.: Indian Ocean experiment: An integrated analysis of the climate forcing and effects of the great Indo-Asian haze, *J. Geophys. Res.*, 106, 28371–28398, 2001.
- Renard, J.-B., Worms, J.-C., Lemaire, T., Hadamcik, E., and Huret, N.: Light scattering by dust particles in microgravity: polarization and brightness imaging with the new version of the PROGRA2 instrument, *Appl. Optics*, 41, 609–618, 2002.
- Renard, J.-B., Brogniez, C., Berthet, G., Bourgeois, Q., Gaubicher, B., Chartier, M., Balois, J.-Y., Verwaerde, C., Auriol, F., Francois, P., Daugeron, D., and Engrand, C.: Vertical distribution of the different types of aerosols in the stratosphere: Detection of solid particles and analysis of their spatial variability, *J. Geophys. Res.*, 113, D21303, doi:10.1029/2008JD010150, 2008.
- Renard, J.-B., Thauray, C., Mineau, J.-L., and Gaubicher, B.: Small-angle light scattering by airborne particulates: Environnement- S. A. continuous particulate monitor, *Meas. Sci. Technol.*, 21, 931–939, doi:10.1088/0957-0233/21/8/085901, 2010a.

10027

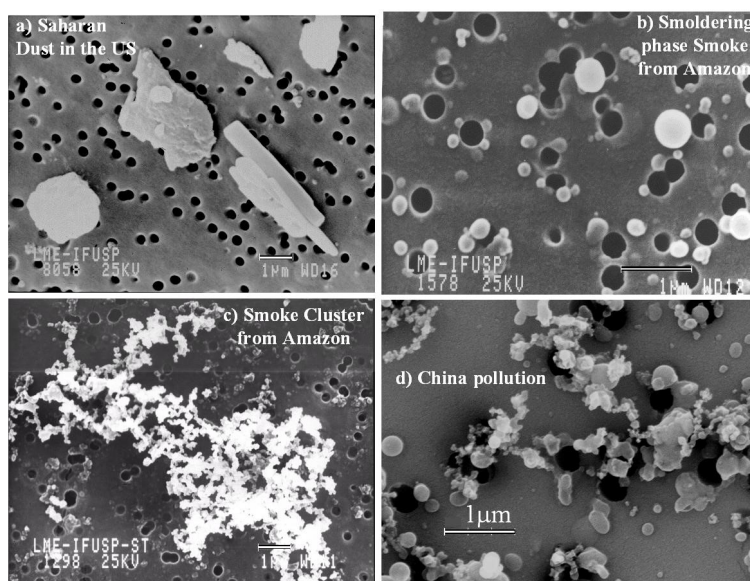
- Renard, J.-B., Berthet, G., Salazar, V., Catoire, V., Tagger, M., Gaubicher, B., and Robert, C.: In situ detection of aerosol layers in the middle stratosphere, *Geophys. Res. Lett.*, 37, L20803, doi:10.1029/2010GL044307, 2010b.
- Renard, J.-B., Dulac, F., Berthet, G., Lurton, T., Vignelles, D., Jégou, F., Tonnelier, T., Thauray, C., Jeannot, M., Couté, B., Akiki, R., Verdier, N., Mallet, M., Gensdarmes, F., Charpentier, P., Mesmin, S., Duverger, V., Dupont, J. C., Elias, T., Crenn, V., Sciare, J., Giacomoni, J., Gobbi, M., Hamonou, E., Olafsson, H., Dagsson-Waldhauserova, P., Camy-Peyret, C., Mazel, C., Décamps, T., Piringer, M., Surcin, J., and Daugeron, D.: LOAC: a small aerosol optical counter/sizer for ground-based and balloon measurements of the size distribution and nature of atmospheric particles – Part 2: First results from balloon and unmanned aerial vehicle flights, *Atmos. Meas. Tech. Discuss.*, 8, 10057–10096, doi:10.5194/amtd-8-10057-2015, 2015
- Rosen, J. M.: The vertical distribution of dust to 30 kilometers, *J. Geophys. Res.*, 69, 4673–4676, 1964.
- Ryder, C. L., Highwood, E. J., Rosenberg, P. D., Trembath, J., Brooke, J. K., Bart, M., Dean, A., Crosier, J., Dorsey, J., Brindley, H., Banks, J., Marsham, J. H., McQuaid, J. B., Sodemann, H., and Washington, R.: Optical properties of Saharan dust aerosol and contribution from the coarse mode as measured during the Fennec 2011 aircraft campaign, *Atmos. Chem. Phys.*, 13, 303–325, doi:10.5194/acp-13-303-2013, 2013.
- Salazar, V., Renard, J.-B., Hauchecorne, A., Bekki, S., and Berthet, G.: A new climatology of aerosols in the middle and upper stratosphere by alternative analysis of GOMOS observations during 2002–2006, *Int. J. Remote Sens.*, 34, 4986–5029, doi:10.1080/01431161.2013.786196, 2013.
- Shaw, G. E., Reagan, J. A., and Herman, B. M.: Investigations of atmospheric extinction using direct solar radiation measurements made with a multiple wavelength radiometer, *J. Appl. Meteorol.*, 12, 374–380, 1973.
- Shi, J. P., Khan, A. A., and Harrison, R. M.: Measurements of ultrafine particle concentration and size distribution in the urban atmosphere, *Sci. Total Environ.*, 235, 51–64, 1999.
- Singh, V. P., Gupta, T., Tripathi, S. N., Jariwala, C., and Das, U.: Experimental study of the effects of environmental and fog condensation nuclei parameters on the rate of fog formation and dissipation using a new laboratory scale fog generation facility, *Aerosol Air Qual. Res.*, 11, 140–154, 2011.

10028

Table 2. Conditions of measurements for evaluation exercises

Campaign	Location	Date	Installation	Instruments for validation
ParisFog	SIRTA Observatory, Palaiseau (France)	Nov 2012–Apr 2013 Sep 2013–Jan 2014	Continuous ground measurements	– WELAS counter – Fog monitor counter – Scanning Mobility Particle Sizer (SMPS)
Cloud measurements	Puy de Dôme (France)	May 2013	Continuous ground measurements	Well-known atmospheric conditions for the topology identification
ChArMEX	Minorca (Spain)	17 Jun 2013	Tropospheric pressurized balloon	Well-known atmospheric conditions for the topology identification
ChArMEX	Ile du Levant (France)	22 Jul 2013	Tropospheric pressurized balloon	Well-known atmospheric conditions for the topology identification
ChArMEX	Minorca (Spain)	15 Jun 2013–2 Jul 2013	Continuous ground measurements	HHPC-6 counter
ChArMEX	Minorca (Spain)	16 and 17 Jun 2013	Meteorological sounding balloon flights	Well-known atmospheric conditions for the topology identification
ChArMEX	Minorca (Spain)	16 and 19 Jun 2013	Meteorological and pressurized tropospheric balloon flights	WALI lidar
QAIDOMUS	Orléans (France)	Sep–Nov 2013	Indoor air	TEOM microbalance
VOLTAIRE-LOAC	Reykjavik (Iceland)	7 Nov 2013	Meteorological balloon flight	Well-known atmospheric conditions for the topology identification
Observatoire Atmosphérique Generali	Paris (France)	Jan–Apr 2014	Permanent measurements on tethered balloon (at ground and up to an altitude of 270 m)	– TEOM microbalances (Airparif air quality network) – Well-known atmospheric conditions for the topology identification
SIRTA5 campaign	Gif-sur-Yvette (France)	3–13 Feb 2014	Continuous ground measurements at SIRTA	– Grimm counter – HHPC-6 counter – SMPS

10031

**Figure 1.** Scanning electron microscope image of ambient air aerosols (courtesy Jose Vanderlei Martins, Institute of Physics of the University of Sao Paulo, Brazil).

10032

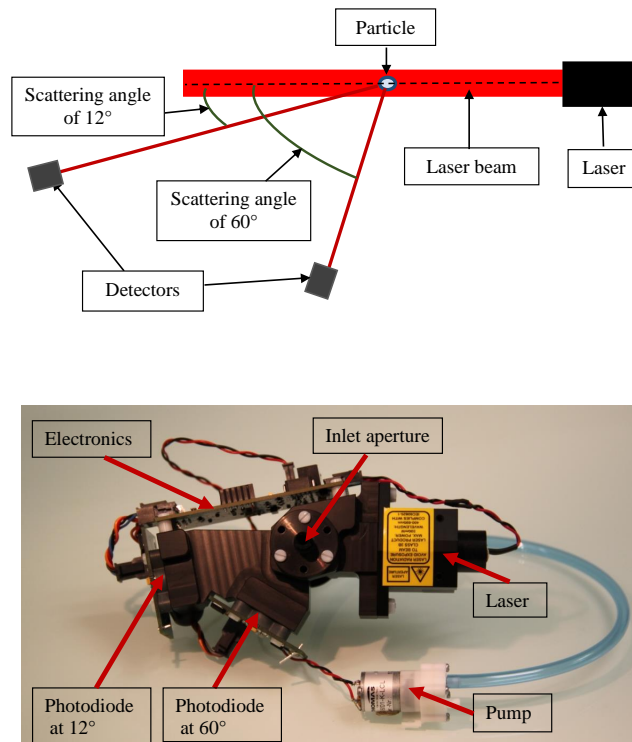


Figure 2. The LOAC instrument; upper panel: principle of measurement; lower panel: picture of the instrument (the inlet tube is not presented here).

10033

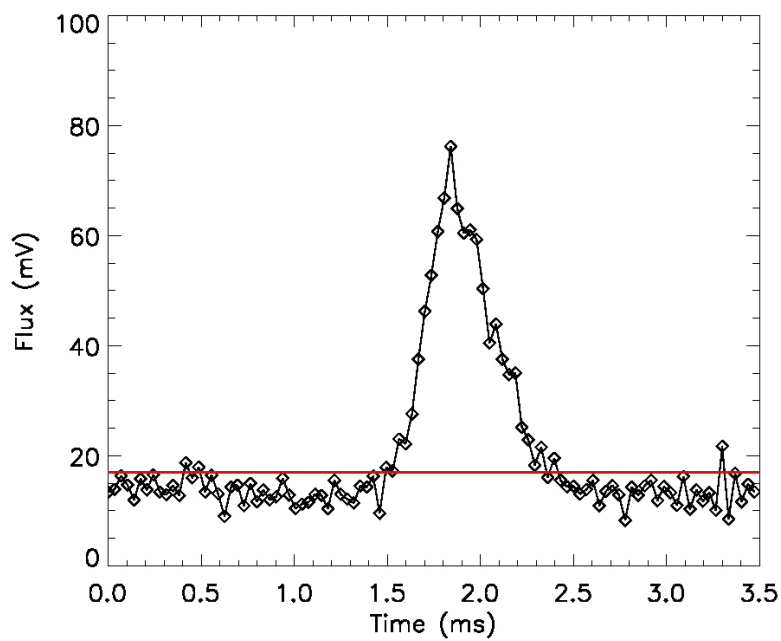


Figure 3. Example of the flux scattered by ambient air particles while crossing the laser beam. The red line corresponds to the threshold for the peak detection. When a particle is detected, the signal must return back below the threshold to allow the detection of the next one.

10034

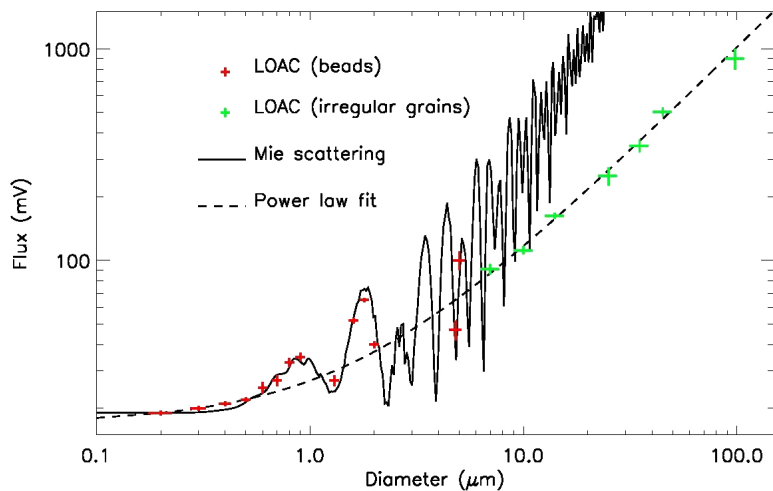


Figure 4. Calibration curve of the scattered flux at the 12° channel as a function of particle diameter. Beads were used in the 0.2–5.0 μm range; irregular grains selected by sifters were used for the largest size. The offset due to the electronic dark current and high frequency noise of the detector were added to the calculations; thus the curve asymptotically decreases with decreasing size to this offset value. The Mie calculations were conducted for the LOAC field of view. The difference between the Mie scattering calculations and LOAC measurements for diameters greater than 5 μm is due to the small aperture of the field of view coupled with the roughness of the particle shapes; the measurement curve is fitted by a power law (adding an offset of 17 mV).

10035

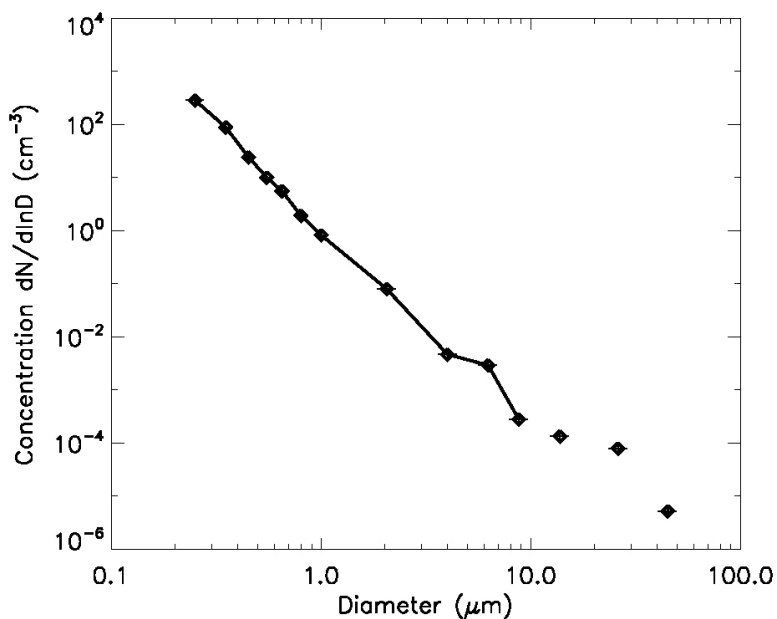


Figure 5. Typical size distribution in a suburban ambient air with carbon particles (Palaiseau, South of Paris) on 14 October 2013 during ParisFog campaign; the data are integrated during 15 min; the last points are not related because of zero concentration measured between them.

10036

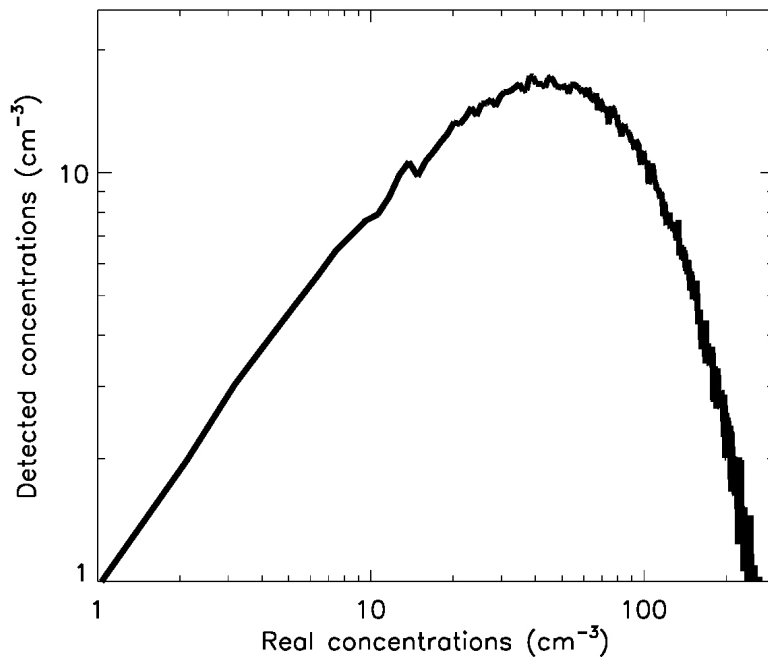


Figure 6. Monte-Carlo modelling for the response of the counting system for particles larger than 1 μm . The response is almost linear up to 10 particles per cm^3 , and decreases for large concentrations.

10037

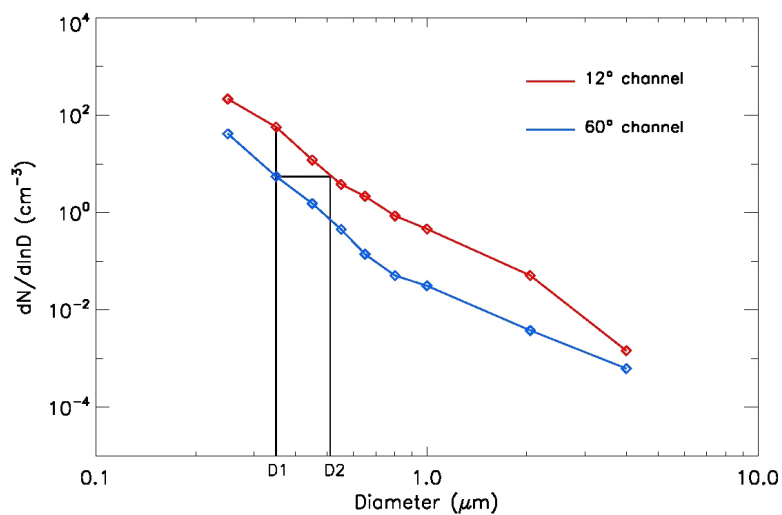


Figure 7. Principle of the determination of the “speciation index” $D2/D1$ (the example presented here uses real measurements).

10038

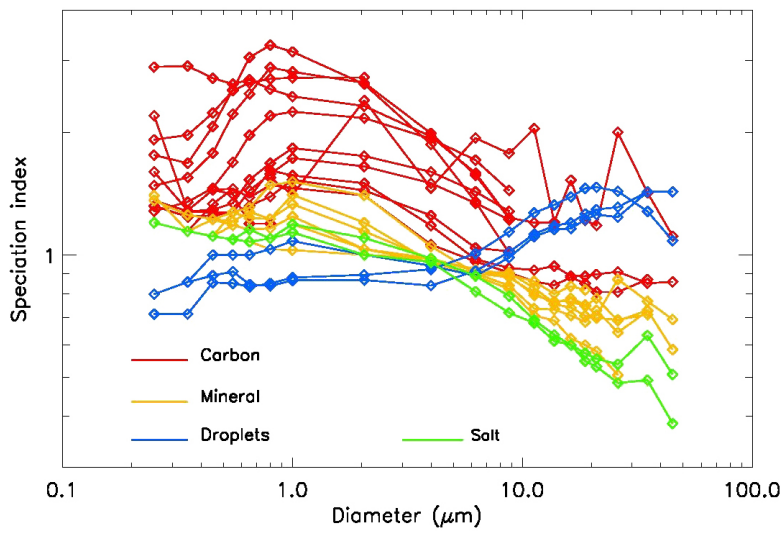


Figure 8. Evolution of the speciation index with diameter for various families of samples; measurements were conducted in laboratory with LOAC using pure samples.

10039

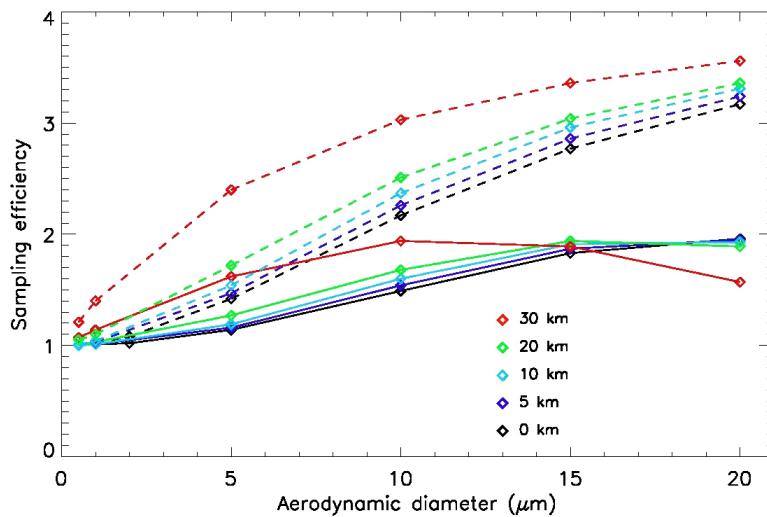


Figure 9. Efficiency of the sampling line at different altitudes from the surface up to 30 km; dashed lines: isoaxial conditions; full lines: 30° deviation from isoaxial conditions.

10040

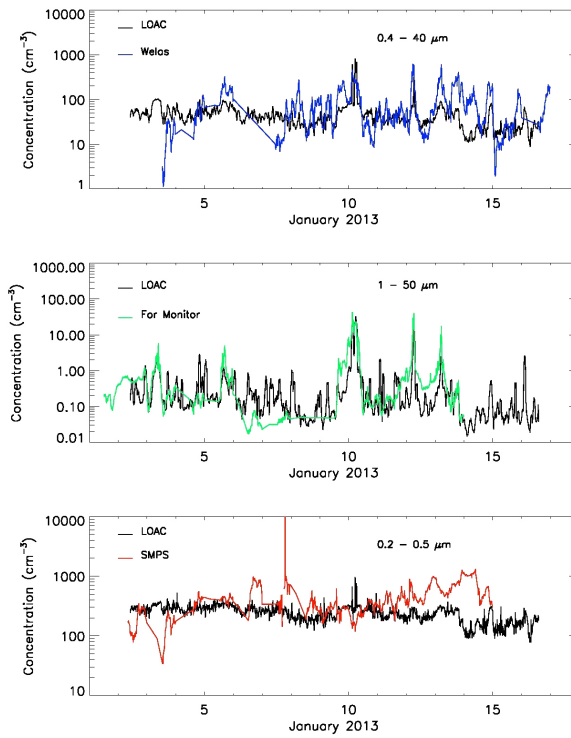


Figure 10. Cross-comparison of LOAC with 3 other instruments (WELAS, Fog Monitor and SMPS) for the total concentrations of aerosols in the size range domain in common, during the ParisFog campaign south of Paris. The LOAC uncertainties are of $\pm 15\%$.

10041

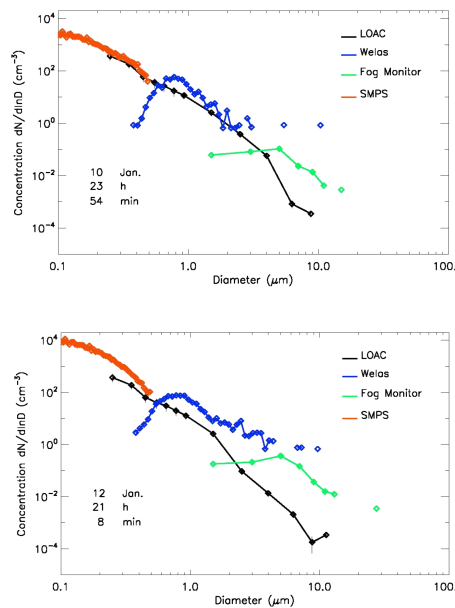


Figure 11. Cross-comparison of the 4 instruments during background conditions, in case of good agreement for the total concentrations measurements, during the ParisFog campaign. Upper panel: 10 January 2013, good agreement between the instruments; lower panel: 12 January 2013, poor agreement. The LOAC uncertainties are of $\pm 15\%$. The WELAS probably underestimates sub- μm particles (Heim et al., 2008).

10042

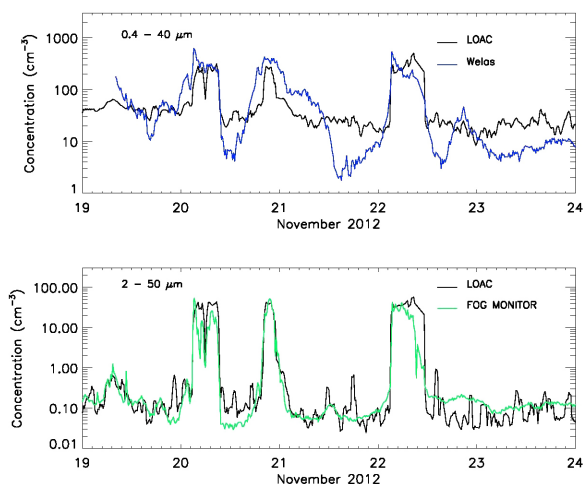


Figure 12. Cross-comparison of LOAC with 2 other instruments (WELAS and Fog Monitor) for the total concentrations of aerosols in the size range domain in common, during the ParisFog campaign. The LOAC uncertainties are of $\pm 15\%$.

10043

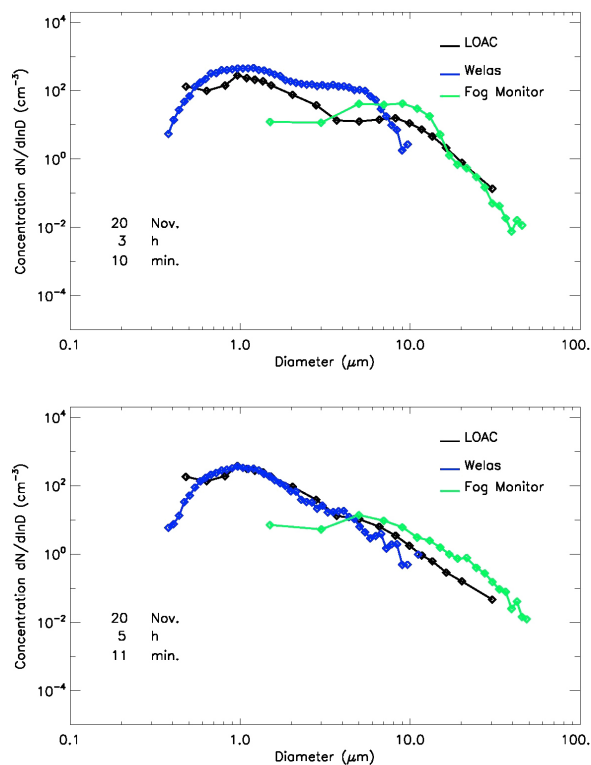


Figure 13. Cross-comparison of the 3 instruments at the beginning of the fog event (top) and at the end (bottom), during the ParisFog campaign on 20 November 2012 during a fog event. The LOAC uncertainties are of $\pm 15\%$. The WELAS probably underestimates sub- μm particles.

10044

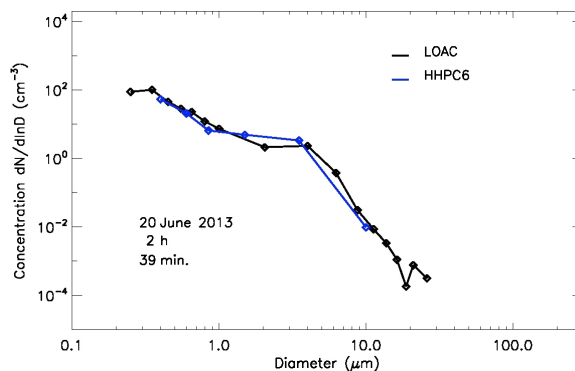


Figure 14. Example of size distribution for LOAC and HHPC-6 during an event of solid particles during the ChArMEx campaign at Minorca on 20 June 2013.

10045

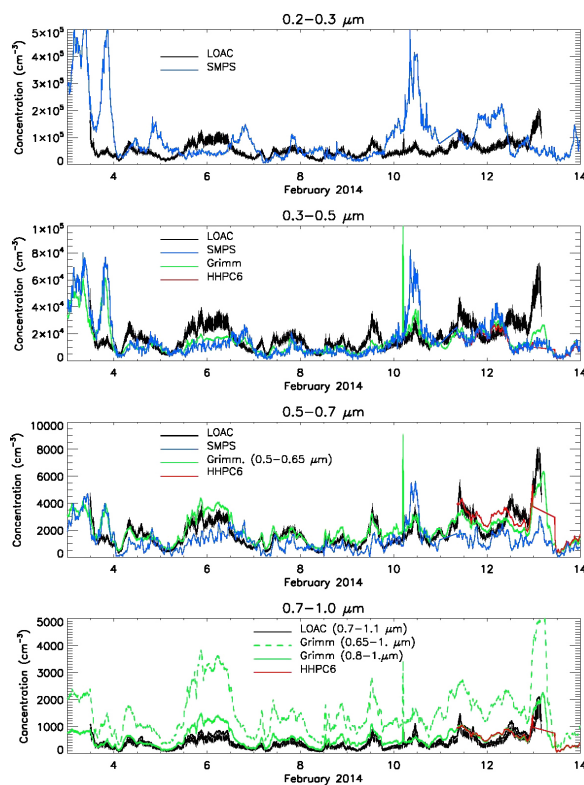


Figure 15. Comparison (in linear scale) between the ambient air measurements obtained during the campaign at the SIRTA-5 station South of Paris.

10046

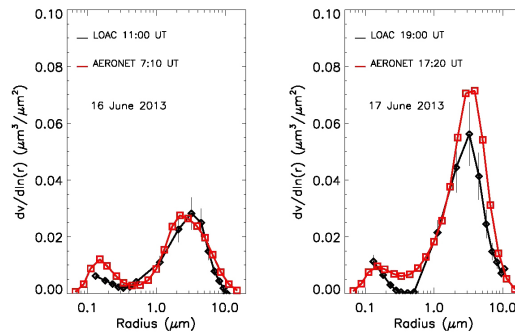


Figure 16. Comparison between integrated LOAC measurements from vertical profiles obtained under meteorological balloons and AERONET measurements during an African dust transport event during the ChArMEx 2013 campaign (note that the LOAC data are given in radius to match the AERONET format).

10047

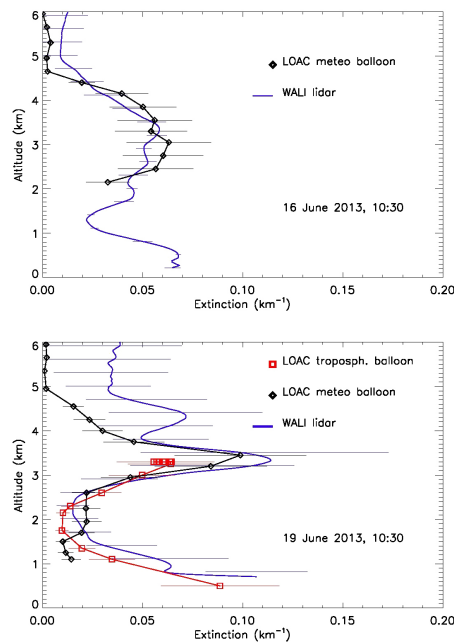


Figure 17. Extinction profiles of the WALI lidar and extinction profiles calculated from LOAC measurements under meteorological and pressurized tropospheric balloons, from Minorca Island during the ChArMEx campaign.

10048

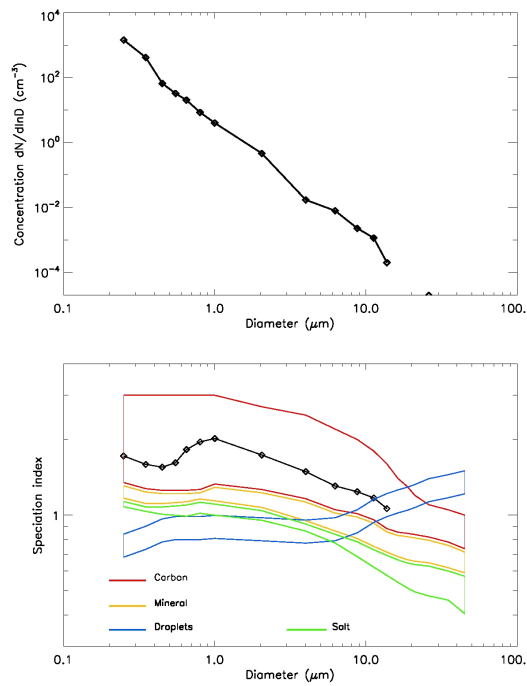


Figure 18. Example of the detection of carbon particles in urban air, in South-West of Paris on 29 December 2013 around 07:30 UT, at the “Observatoire Atmosphérique General”; upper panel: size distribution; lower panel: topology.

10049

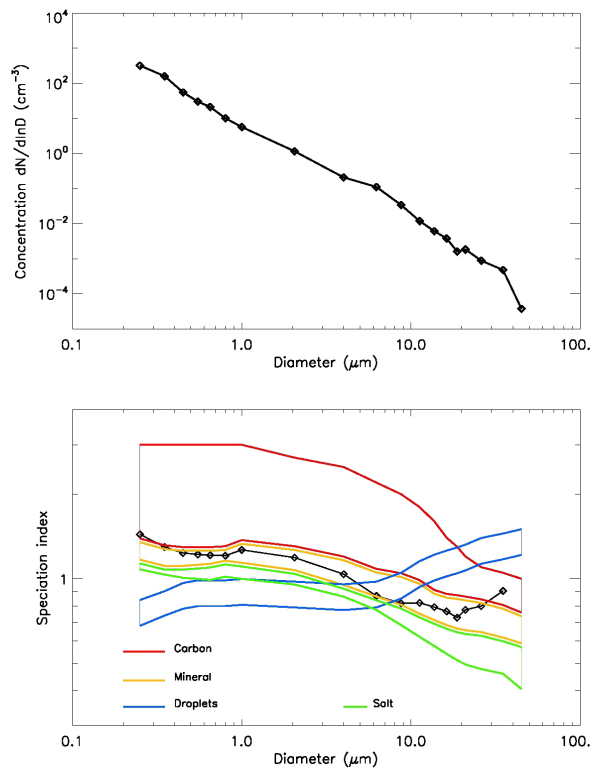


Figure 19. Example of the detection of sand particles above Mediterranean Sea (close to Minorca) from a drifting pressurized tropospheric balloon on 17 June 2013 around 14:30 UT at an altitude of 2050 m, during the ChArMEx campaign; upper panel: size distribution; lower panel: topology.

10050

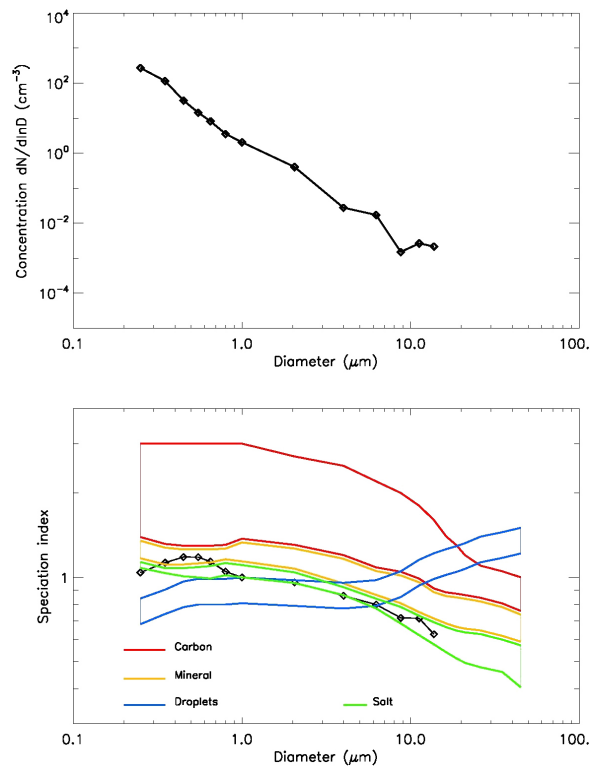


Figure 20. Example of the detection of salt particles above Mediterranean Sea (close to Minorca, Spain) from balloon on 22 July 2013 at 21:25 UT at an altitude of 275 m during the ChArMEx campaign; upper panel: size distribution; lower panel: topology.

10051

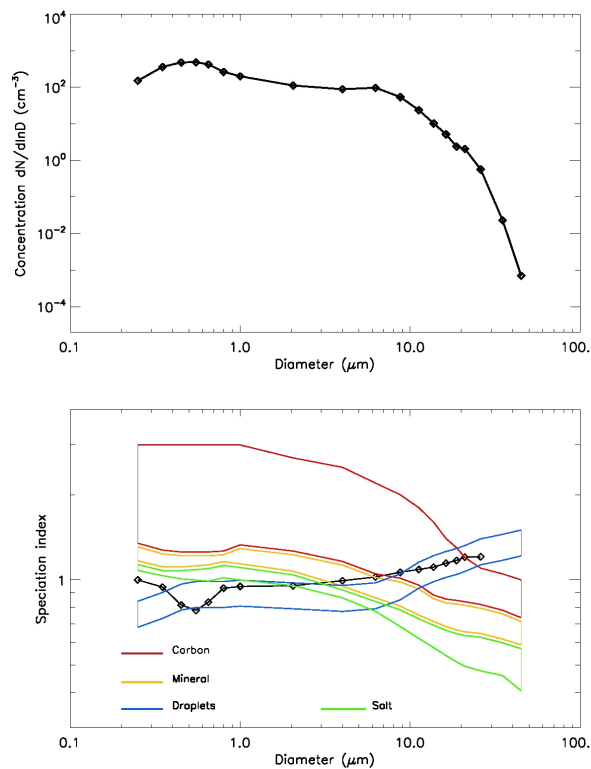


Figure 21. Example of measurements inside a cloud at Puy de Dôme observatory (France) on 15 May 2013 at 10:30 UT; upper panel: size distribution; lower panel: topology.

10052

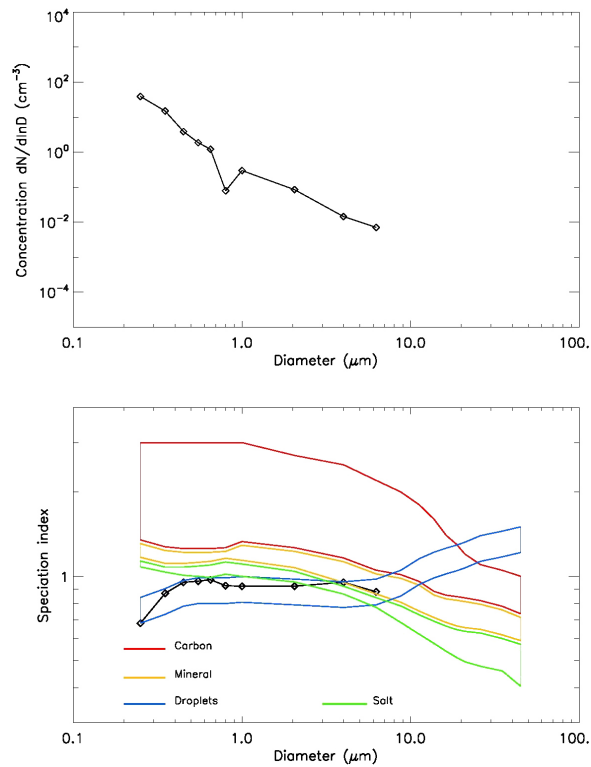


Figure 22. Example of measurements inside a haze or thin cloud at an altitude of 1.2 km during a flight under meteorological balloon from Reykjavik (Iceland) on 7 November 2013 at 12:30 UT; upper panel: size distribution; lower panel: topology.

10053

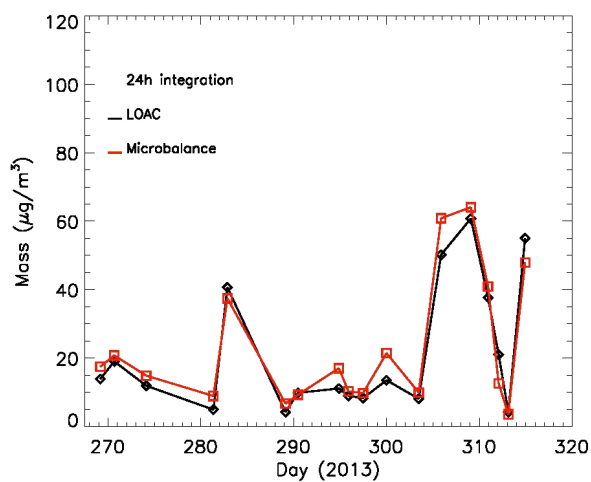


Figure 23. Comparison of coincident LOAC and TEOM microbalance measurement in indoor air (averaged over 24 h); particles have been injected with various concentrations to document a large range of mass concentration.

10054

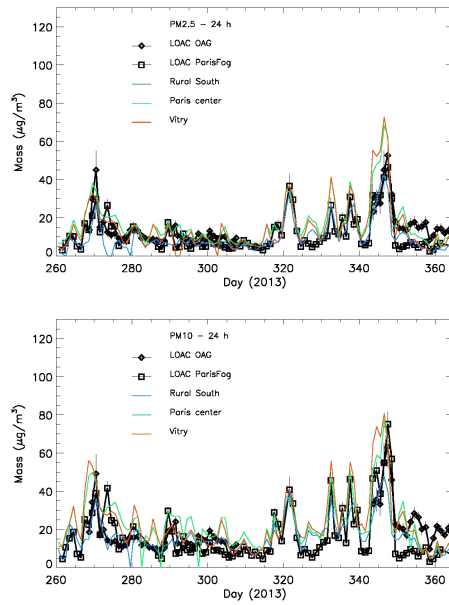


Figure 24. $PM_{2.5}$ (upper panel) and PM_{10} (lower panel) LOAC mass concentrations measurements in 2013 during the ParisFog campaign at SIRTA Observatory in Palaiseau, South of Paris, and at the Observatoire Atmosphérique Generali(OAG) in the South-West of Paris, and comparison with reference TEOM data from the Airparif air quality monitoring network.

10055

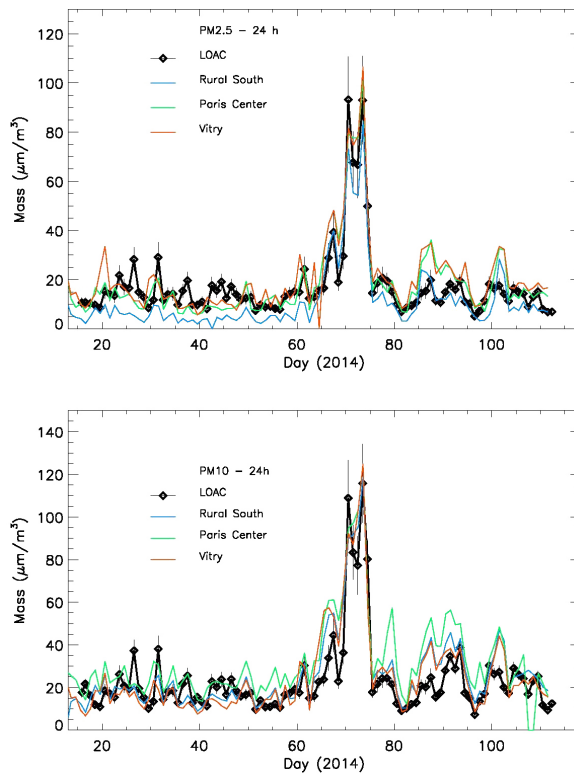


Figure 25. $PM_{2.5}$ (upper panel) and PM_{10} (lower panel) LOAC mass concentrations measurements in 2014 at the “Observatoire Atmosphérique Generali” (South-West of Paris) and comparison with reference TEOM data from the Airparif air quality monitoring network.

10056